Contents lists available at ScienceDirect

Biochemistry and Biophysics Reports

Rosolic acid as a novel activator of the Nrf2/ARE pathway in arsenic-induced male reproductive toxicity: An *in silico* study

Anirban Goutam Mukherjee , Abilash Valsala Gopalakrishnan [*]

Department of Biomedical Sciences, School of Bio-Sciences and Technology, Vellore Institute of Technology, Vellore, Tamil Nadu, 632014, India

A B S T R A C T

Male reproductive toxicity as a result of arsenic exposure is linked with oxidative stress and excessive generation of reactive oxygen species (ROS). It leads to an imbalance between ROS production and antioxidant defense mechanisms ultimately resulting in male infertility. The nuclear factor erythroid 2 (NFE2)-related factor 2 (Nrf2) is a transcription factor that responds to cellular stressors controlling the oxidative state, mitochondrial dysfunction, inflammation, and proteostasis. This study aims to investigate the potential of Rosolic acid (ROA) to act as a novel Nrf2 activator by mitigating oxidative stress to combat arsenic-induced male reproductive toxicity. The protein and ligands were prepared in the BIOVIA Discovery Studio, followed by protein-ligand docking using auto dock vina integrated with the PyRx-Virtual Screening Tool. Then the ADME properties were analyzed using the SwissADME tool to get a clear idea about the physicochemical properties, lipophilicity, water solubility, pharmacokinetics, and drug likeliness of ROA. It was followed by molecular dynamics simulation (MDS) studies using GROMACS. The 3D and 2D interaction maps revealed the interactions of Keap 1 with ROA. Keap1-ROA complex was found to have a binding energy of −7.8 kcal/mol. ROA showed 0 violations for Lipinski and 0 alerts each for PAINS and Brenk and a bioavailability score of 0.55. The BOILED-Egg representation showcases that ROA is predicted as passively crossing the blood-brain barrier (BBB). The MDS described 2FLU-ROA as a stable system. This work portrays that ROA can be a potent Nrf2 activator by exhibiting an inhibitory activity against the Keap1 protein and thus mitigating oxidative stress in arsenic-induced male reproductive toxicity.

1. Introduction

Oxidative stress is a state where the cell's antioxidant defense system is unable to cope with the excessive production of reactive oxygen species (ROS) leading to an oxygen paradox. ROS are extremely reactive oxidizing free radical agents including superoxide anions ($O_2 \bullet$), hydrogen peroxide (H_2O_2), peroxyl ($ROO\bullet$), and hydroxyl ($OH\bullet$) radicals [1]. Free radicals are necessary for cellular functions, but at higher levels, they can disrupt vital metabolic processes [2]. Oxidative stress is a primary factor that leads to dysfunctional sperm and plays a significant role in the development of male infertility [3]. This is due to the negative impact it has on both the physical and functional integrity of spermatozoa [4–6]. The primary origins of ROS in sperm are activated leukocytes present in the seminal plasma and the mitochondria inside the spermatozoa. Abundant data indicates that damage to spermatozoa caused by ROS is a significant factor in the development of infertility in 30–80% of infertile men [1,7,8]. Optimal amounts of ROS are necessary

for various redox-sensitive physiological processes, including sperm capacitation and hyperactivation. However, too high levels of ROS hinder the fluidity and permeability of sperm membranes [9]. The precise cause of the decrease in sperm function due to oxidative stress is not yet fully understood. However, it is primarily believed to be caused by the damaging effects of peroxidation on the axoneme and the reduction of intracellular ATP levels. This is followed by the production of 4-hydroxynonenal and malondialdehyde as a result of the oxidation of lipid membrane components, as well as the fragmentation of both nuclear and mitochondrial DNA [8–10].

Arsenic exposure triggers the production of ROS inside cells, which in turn bring about various alterations in cell behavior by affecting signaling pathways and epigenetic modifications, or by directly causing oxidative damage to molecules [11–13]. Arsenic induces changes in mitochondrial structure and function [14,15]. The accumulation of arsenic in the male reproductive organs is extensively reported and leads to disruptions in the physiological processes associated with producing

---

viable spermatozoa, including steroidogenesis, spermatogenesis, and sperm maturation [16]. Male individuals exposed to arsenic commonly experience many changes, such as a reduction in testicular weight, lower levels of testosterone in the blood, reduced sperm count, diminished viability of sperm, and decreased sperm motility [17–19]. The testis has a role in the production of steroids, specifically testosterone, which is synthesized by Leydig cells. Arsenic causes reproductive dysfunction by reducing testosterone production and disrupting the functioning of androgen receptors at the transcriptional level. Arsenic exposure leads to oxidative damage, which in turn disrupts the morphology and functionality of Leydig cells [16,20–23].

Arsenic-induced inhibition of glycolysis disrupts the ability of spermatogonial stem cells to renew themselves and regenerate, as demonstrated by Park and Pang in 2021 [24]. Autophagy is a cellular process that involves recycling damaged proteins and organelles by breaking them down through the lysosomal route, hence providing self-protection to the cells. Arsenic exposure can lead to autophagy in the spermatogenic lineage by causing cellular redox imbalance and damaging mitochondria [25]. Arsenic disrupts the process of spermiogenesis in the stage where round spermatids are produced by causing disarray in the elongation of spermatids. It, in turn, leads to changes in the expression of the DDX25 gene and impacts the formation of the axoneme of the flagellum and the development of the acrosome [26,27]. Arsenic can decrease the activity of transmembrane proteins in the blood-testis barrier (BTB), resulting in disruption of cell communication and impairment of spermatogenesis [28].

The Nrf2 signaling pathway controls the expression of more than 200 genes, which include antioxidant enzymes, cytoprotective proteins, and xenobiotic transporters. In a quiescent condition, Nrf2, a member of the cap 'n' collar family of basic leucine zipper proteins with seven highly conserved domains, is held in the cytoplasm by Kelch-like ECH-Associated Protein 1 (Keap1) and marked for degradation through ubiquitination. This degradation occurs in the cytoplasm through the Cul3-Rbx1 E3 ubiquitin ligase system [29,30]. Nrf2 controls the antioxidant response pathway by binding to antioxidant response elements (AREs) in the promoters of antioxidant genes. These sequences are *cis*-acting enhancers. Nrf2 forms a regular binding interaction with Keap1 in the cytosol, leading to the degradation of Nrf2. When there is oxidative stress or the presence of electrophiles, Keap1 undergoes modification. This modification leads to a change in the shape of Keap1, which reduces the degradation of Nrf2 that depends on Keap1 [31]. This leads to the activation and stabilization of Nrf2, which then moves into the nucleus. In the nucleus, Nrf2 forms a complex with small musculoaponeurotic fibrosarcoma (sMAF) proteins and other co-transcriptional factors. This complex binds to the ARE and starts the transcription of antioxidant enzymes [30,32,33]. A more detailed idea about the Nrf2 signaling pathway can be obtained from our previously published work [34].

Abnormal expression of Nrf2 has been linked to multiple diseases. Dysregulation of the Nrf2 signaling pathway is associated with cardiovascular disease, diabetes, neurodegenerative disease, mental disorders, and cancer [35]. Although initially identified as a target for chemopreventive compounds that aid in the prevention of cancer and other diseases, mounting data has confirmed that the Nrf2 pathway has a significant role in promoting cancer progression, metastasis, and resistance to treatment. Nrf2 has been found to have new roles in regulating metabolism and other crucial cellular functions, confirming its status as a pleiotropic transcription factor [36]. In an earlier study, we explored the complexities of abnormalities in the Nrf2 pathway in cancer, the possible consequences of unregulated Nrf2 activity, and therapeutic approaches to regulate the Keap1-Nrf2 pathway [34].

The Nrf2 system, consisting of Nrf2 and its associated genes, is expressed in the testis and is crucial in protecting against damage to the testicular tissue [37]. They play a crucial role in controlling the BTB and the functioning of testicular tissue [38]. Moreover, the decreased expression of Nrf2 in the testes of mice and human sperm cells is associated with impaired sperm production due to diabetes and smoking [39,40]. Therefore, Nrf2 could be a prominent biomarker for predicting male infertility [41]. Wajda et al. (2016) [38] have suggested that Nrf2 is crucial in preventing oxidative damage to spermatogenesis. Nrf2 safeguards the testis against oxidative stress by actively participating in cellular antioxidant defense [38,42].

Nrf2 inhibitors in the testis could enhance oxidative stress, leading to negative consequences that may damage the Nrf2 signaling pathway and cause testicular dysfunction [41,43,44]. Given this information, Nrf2 could be a promising treatment candidate for addressing oxidative stress in the testicles and improving the antioxidant balance [41,45]. Nrf2 activators are promising drugs for enhancing antioxidant capacity and combating excessive oxidative stress. Activating antioxidant enzymes, specifically via Nrf2, is a primary approach in advancing antioxidant therapy. The primary mechanism by which small molecules such as polyphenols exert their effects is through the induction of antioxidant enzymes, which is mediated by the Nrf2 signaling [41,46–48]. However, there may be certain obstacles that could restrict the implementation of this treatment approach. The therapeutic prospects may be hindered by the low bioavailability of drugs (namely Nrf2 activators) caused by the presence of the BTB. Nevertheless, nanocarriers improve the capacity of therapeutic agents to be absorbed by the body and show significant promise in crossing the BTB [41].

Rosolic acid (ROA), commonly referred to as aurin, is a polyphenol derived from the rhizome of *Plantago asiatica* L. Numerous studies have demonstrated its cytoprotective properties, mainly attributed to its notable capacity to enhance Heme Oxygenase-1 (HO-1) levels, particularly in endothelial cells [49–51]. This study explores the potential of ROA to mitigate oxidative stress-induced male reproductive toxicity via an *in-silico* approach. We think this study can be crucial in addressing the issue of ROS-induced male reproductive damage as a result of arsenic toxicity. As far as we know, this study is the first to examine the importance of ROA as a therapeutic strategy in male reproductive toxicity.

2. Materials and methods

2.1. Preparation of the protein structure

The 3D conformation of the Keap1 protein was obtained from the Protein Data Bank (PDB) using the PDB ID: 2FLU. The protein preparation steps, including deleting the water molecules and unwanted chains, were carried out using the BIOVIA Discovery Studio. The polar hydrogens were also added, and the protein was saved in the pdb format.

2.2. Preparation of the ligands

The 3D conformers of ROA (PubChem CID: 5100), Keap1-Nrf2-IN-3 commonly known as 5RB (PubChem CID: 126754534), and Curcumin (PubChem CID: 969516) were obtained from the PubChem database in SDF format. Keap1-Nrf2-IN-3 (5RB) and Curcumin (CUR) were taken as two controls for the study. Keap1-Nrf2-IN-3 is a very commonly known Keap1:Nrf2 protein−protein interaction inhibitor and CUR has been widely known as a common antioxidant and an inhibitor of Keap1 protein [52–54]. CUR has also been found to be highly beneficial in treating oxidative stress-induced male reproductive toxicity [40,55,56]. Hence we selected 5RB and CUR as the controls for further studies. Energy minimization for ROA, 5RB, and CUR was performed using PyRx 0.8 software.

2.3. Docking studies

The interaction of the ligands ROA, 5RB, and CUR with Keap1 protein was analyzed using the PyRx 0.8 software with the integrated Autodock Vina algorithm. The BIOVIA Discovery Studio Visualizer was used to visualize the docking results.
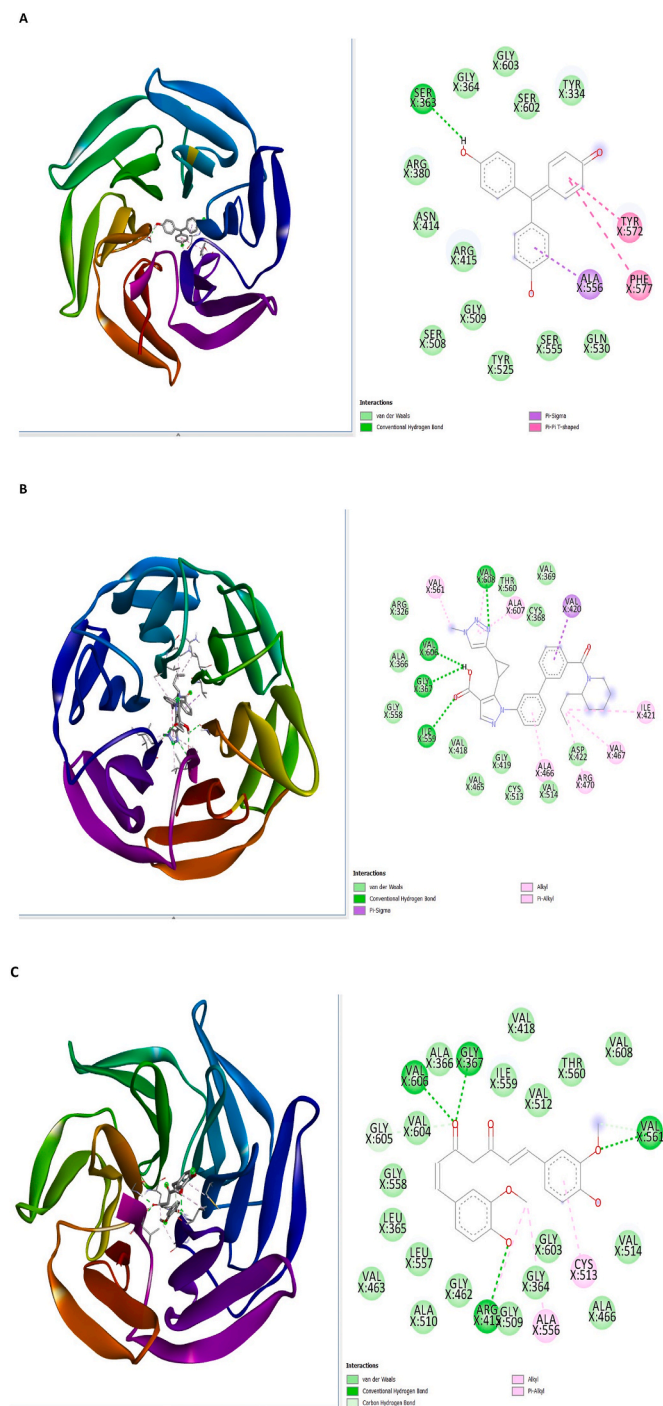
Fig. 1. 3D and 2D illustration of the docking results. Fig. 1A portrays the docking of ROA with the Keap1 protein (PDB ID: 2FLU). Fig. 1B represents the docking of 5RB with 2FLU whereas Fig. 1C showcases the docking of CUR with 2FLU.

2.4. ADME properties

ROA, 5RB, and CUR underwent evaluation of drug-like features using the SwissADME software [57]. Examining the ADME properties provides crucial insights into the behavior, and fate of a drug candidate within the human body.

Table 1

Results of the docking studies. This table describes the binding affinity, different types of bonds, and various amino acid residues involved in docking ROA, 5RB, and CUR with the protein Keap1(PDB ID: 2FLU). The amino acid residues involved in the formation of conventional hydrogen bonds are marked in **bold**.

Protein-ligand	Binding affinity (kcal/mol)	Different types of bonds	Amino acids
Keap1(PDB ID: 2FLU)-ROA (PubChem CID: 5100)	−7.8	Van der Waals, Conventional hydrogen bond, Pi-Pi T-shaped, Pi-Sigma	**SER363**, ALA556, TYR572, PHE577, TYR334, SER602, GLY603, GLY364, ARG380, ASN414, ARG415, GLY509, SER508, TYR525, SER555, GLN530
Keap1(PDB ID: 2FLU)-5RB (PubChem CID: 126754534)	−9.6	Conventional hydrogen bonding, Pi-sigma, Alkyl, Pi-Alkyl, and van der Waals	VAL420, VAL369, CYS368, ALA607, THR560, **VAL608**, VAL561, ARG326, **VAL606**, ALA366, **GLY367**, GLY558, **ILE559**, VAL418, VAL465, GLY419, CYS513, ALA466, VAL514, ASP422, ARG470, VAL467, ILE421
Keap1(PDB ID: 2FLU)-CUR (PubChem CID: 969516)	−8.6	Conventional hydrogen bonding, Carbon Hydrogen bond, Alkyl, Pi-Alkyl, and van der Waals forces	**VAL561**, VAL608, THR560, VAL512, ILE559, VAL418, **GLY367**, ALA366, **VAL606**, VAL604, GLY605, GLY558, LEU365, VAL463, LEU557, ALA510, GLY462, **ARG415**, GLY509, GLY364, GLY603, ALA556, CYS513, ALA466, VAL514

2.5. Molecular dynamics

The docked complexes of ROA, 5RB, and CUR with 2FLU were critically analyzed using MDS. The pdb2gmx module in GROMACS was utilized to add hydrogens to the heavy atoms. Using the steepest descent algorithm, the prepared systems were first vacuum minimized for 1500 steps. Using a simple point-charge water model, the structures were solvated in a cubic periodic box. The intricate systems were balanced by introducing the necessary amount of Na^+ and Cl^- counter ions to maintain a salt concentration of 0.15 M [58]. Each structure obtained from the NPT (number of atoms in the system, pressure of the system and temperature of the system) equilibration phase underwent a 200 ns simulation in an NPT ensemble during the final production run. The molecular Mechanics Poisson-Boltzmann surface area (MM-PBSA) method [59] was used to analyze the binding free energy of ROA, 5RB, and CUR with 2FLU during the simulation period.

3. Results and discussions

3.1. Docking studies

The Keap1-Nrf2 regulatory mechanism is a crucial pathway that protects the human body from oxidative stress. Analyzing the Nrf2 pathway through computational methods offers a great chance to develop a potential treatment for diseases resulting from abnormalities in this pathway [60]. Molecular docking is an economical and easy technique for anticipating molecular interactions. Consequently, we employed this strategy to predict and identify probable inhibitors of Keap1 that can successfully obstruct its binding to Nrf2. The Keap1

Table 2
The comparison of the ADME properties of ROA, 5RB, and CUR.

ADME properties		Molecule		
		Rosolic acid (ROA)	Keap1-Nrf2-IN-3 (5RB)	Curcumin (CUR)
Physicochemical properties	**Molecular Weight (MW) g/mol**	290.31	538.64	368.38
	Formula	$C_{19}H_{14}O_3$	$C_{31}H_{34}N_6O_3$	$C_{21}H_{20}O_6$
	Number of Heavy atoms	22	40	27
	Number of aromatic heavy atoms	12	22	12
	Number of H-bond acceptors	3	6	6
	Number of H-bond donors	2	1	2
	Molar refractivity	86.24	156.29	102.80
	Topological Polar Surface Area (TPSA) Å^2	57.53	106.14	93.06
Lipophilicity	**iLOGP**	2.18	3.61	3.27
	XLOGP3	0.35	4.44	3.20
	WLOGP	3.59	5.05	3.15
	MLOGP	2.59	3.92	1.47
	SILICOS-IT	3.27	3.71	4.04
	Consensus Log $P_{o/w}$	2.40	4.15	3.03
Water solubility	**Log S ESOL**	−2.13	−5.79	−3.94
	Ali	−1.12	−6.39	−4.83
	SILICOS-IT	−4.41	−7.15	−4.45
Pharmacokinetics	**BBB permeant**	Yes	No	No
	P-gp substrate	No	Yes	No
	CYP1A2 inhibitor	No	No	No
	CYP2C19 inhibitor	No	Yes	No
	CYP2C9 inhibitor	No	Yes	Yes
	CYP2D6 inhibitor	No	Yes	No
	CYP3A4 inhibitor	No	Yes	Yes
Druglikeness	**Lipinski**	Yes (0 violation)	Yes (1 violation)	Yes (0 violation)
	Ghose	Yes	No (3 violations)	Yes
	Veber	Yes	Yes	Yes
	Egan	Yes	Yes	Yes
	Muegge	Yes	Yes	Yes
	Bioavailability Score	0.55	0.56	0.55
Medicinal Chemistry	**PAINS alerts**	0	0	0
	Brenk alerts	0	0	2
	Leadlikeness	Yes	No (3 violations)	No (2 violations)

structure (PDB ID: 2FLU) underwent molecular docking and was evaluated for its interaction with ROA, 5RB, and CUR. The capacity of these compounds to disrupt the binding between Keap1 and Nrf2 was assessed. The binding affinity and docking score of these molecules were assessed during screening [61]. The molecular docking analysis examined the interactions between ROA, 5RB, CUR, and Keap1 protein.

We have docked ROA, 5RB, and CUR in the current study with the Keap1 structure (PDB ID: 2FLU). The 3D and 2D interaction diagrams revealed that 16 amino acid residues of Keap 1 formed interactions with ROA, for instance, SER363, ALA556, TYR572, PHE577, TYR334, SER602, GLY603, GLY364, ARG380, ASN414, ARG415, GLY509, SER508, TYR525, SER555, GLN530. Those interactions were facilitated by conventional hydrogen bonds, Pi-Pi T-shaped, Pi-Sigma, and van der Waals forces (Fig. 1A). The complex was found to have a binding energy of −7.8 kcal/mol (Table 1).

The interaction between Keap1 and 5RB demonstrated that 5RB interact with 23 specific amino acid residues of Keap1, including VAL420, VAL369, CYS368, ALA607, THR560, VAL608, VAL561, ARG326, VAL606, ALA366, GLY367, GLY558, ILE559, VAL418, VAL465, GLY419, CYS513, ALA466, VAL514, ASP422, ARG470, VAL467 and ILE421. These interactions were made possible by forming conventional hydrogen bonding, Pi-Sigma, Alkyl, Pi-Alkyl, and van der Waals forces (Fig. 1B). The binding energy of the complex was found to be −9.6 kcal/mol (Table 1).

The interaction between Keap1 and CUR portrayed that CUR interacts with 25 specific amino acid residues of Keap1, including VAL561, VAL608, THR560, VAL512, ILE559, VAL418, GLY367, ALA366, VAL606, VAL604, GLY605, GLY558, LEU365, VAL463, LEU557, ALA510, GLY462, ARG415, GLY509, GLY364, GLY603, ALA556, CYS513, ALA466, and VAL514. These interactions were made possible by forming conventional hydrogen bonding, Carbon Hydrogen bond, Alkyl, Pi-Alkyl, and van der Waals forces (Fig. 1C). The binding energy

of the complex was −8.6 kcal/mol (Table 1).

Therefore it is evident that the binding energy of the 2FLU-ROA complex is near about similar to that of the two positive controls namely the 2FLU-5RB and 2FLU-CUR complexes. Hence we can conclude that ROA holds the potential to act as a Keap1 inhibitor.

3.2. ADME properties

SwissADME is a popular software program for predicting small drug pharmacokinetic characteristics. The Swiss Institute of Bioinformatics developed this software, readily accessible online for academic and scientific use at no cost. SwissADME employs several methods and models to predict crucial pharmacokinetic parameters, including absorption, distribution, metabolism, and excretion (ADME) characteristics of drugs. SwissADME provides a user-friendly interface that enables users to enter chemical structures in several forms, such as SMILES or InChI. The software utilizes advanced algorithms to understand crucial pharmacokinetic characteristics such as lipophilicity (logP), water solubility, drug-likeness, and bioavailability [57,62–65]. SwissADME offers data regarding drug-drug interactions, metabolic stability, and the capacity of a molecule to cross the blood-brain barrier (BBB). In addition, the software provides information on the probable toxicity of chemicals using multiple models. SwissADME utilizes many computational techniques and algorithms to describe these pharmacokinetic characteristics. The mentioned models encompass machine learning models, quantitative structure-activity relationship (QSAR) models, and models that compute the physicochemical properties. The software amalgamates data from several databases and literature sources to augment the precision of its predictions. SwissADME can handle various chemical structures and accurately predict attributes for both small and large molecules. The evaluation of ADME properties gives a complete idea of the various critical characteristics of the molecules [57,62–65].
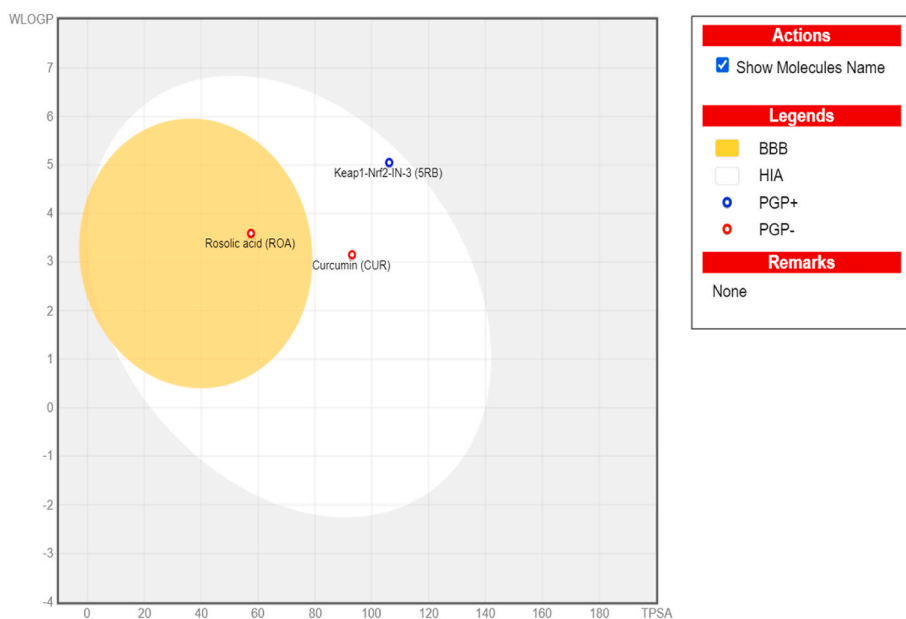
Fig. 2. The BOILED-Egg enables the assessment of HIA and BBB based on the position of the molecules in the WLOGP-versus-TPSA reference system. Here ROA is predicted to passively cross the BBB (in the yolk) and PGP- (red dot). CUR is predicted to not access the brain (in the white) and PGP- (red dot) whereas 5RB was found to be PGP+ (blue dot) and not cross the BBB (in the white). (For interpretation of the references to colour in this figure legend, the reader is referred to the Web version of this article.)

We have comprehensively examined ROA, 5RB, and CUR using the SwissADME software (Table 2).

SwissADME tool predicted the drug-likeness of the proposed Keap1 inhibitors. Among the selected candidates, ROA showed 0 violations for Lipinski and 0 alerts each for PAINS and BRENK. ROA was found to be a BBB permeant and was not found to be a P-glycoprotein (P-gp) substrate. 5RB showed 1 violation for Lipinski, 3 violations for Ghose, and 0 alerts each for PAINS and BRENK. 5RB was not found to be BBB permeant but was found to be a P-gp substrate. CUR showed 0 violations for Lipinski and 2 alerts for BRENK. CUR was found neither to be a BBB permeant nor a P-gp substrate. The bioavailability score of ROA and CUR was found to be 0.55 each whereas it was 0.56 for 5RB.

3.2.1. Graphical output

The BOILED-Egg method concurrently predicts two important ADME parameters: passive gastrointestinal absorption (HIA) and BBB access [62]. Fig. 2 displays a classification plot in the shape of an egg, which consists of two parts: the yolk represents the physicochemical region where BBB permeability is highly likely, and the white represents the physicochemical space with a high likelihood of HIA. Practically, the BOILED-Egg has demonstrated a clear and efficient ability to read and translate into molecular design in several drug development scenarios. The integration of SwissADME includes the addition of P-gp substrate prediction to the graphical output. P-gp substrate is a crucial active efflux mechanism in biological barriers. Furthermore, the points are shaded in blue to indicate that they are anticipated to be actively transported by P-gp (PGP+) and in red to indicate that they are projected not to be substrates of P-gp (PGP-) (Fig. 2) [57,62,63].

3.3. MDS

3.3.1. Root mean square deviation (RMSD)

The RMSD values were assessed over a period of 200 ns to examine the stability of the complexes [66]. 2FLU-ROA complex achieved equilibrium and maintained a uniform distribution during the simulation process. RMSD values showed that the 2FLU-apoprotein (APO) and 2FLU-ROA were steady for 200 ns, portraying the stability of the docked complex throughout the simulation. The average RMSD values for
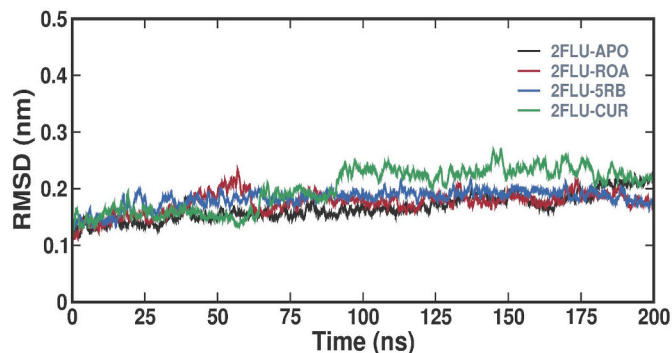

Fig. 3. A comparison of the RMSD values of 2FLU-APO, 2FLU-ROA, 2FLU-5RB, and 2FLU-CUR.

2FLU-APO, 2FLU-ROA, 2FLU-5RB and 2FLU-CUR were found to be 0.16 ±0.02 nm, 0.17±0.01 nm, 0.18±0.01 nm and 0.20±0.03 nm. The results portray that the 2FLU-ROA complex, was stable throughout the simulation without any notable variations (Fig. 3).
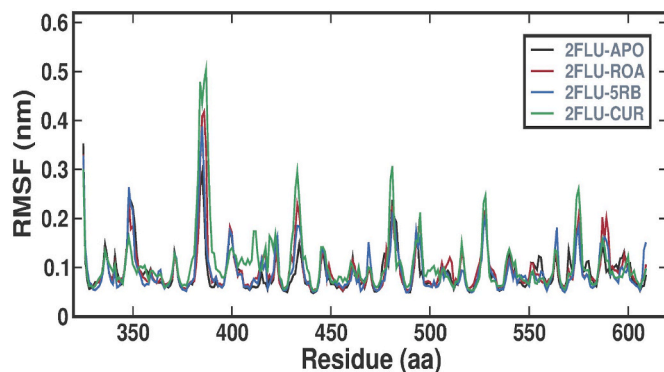

Fig. 4. A comparison of the RMSF values of the 2FLU-APO, 2FLU-ROA, 2FLU-5RB, and 2FLU-CUR complex.
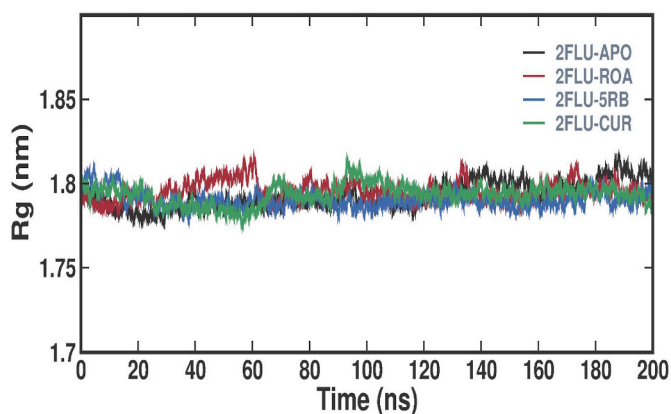
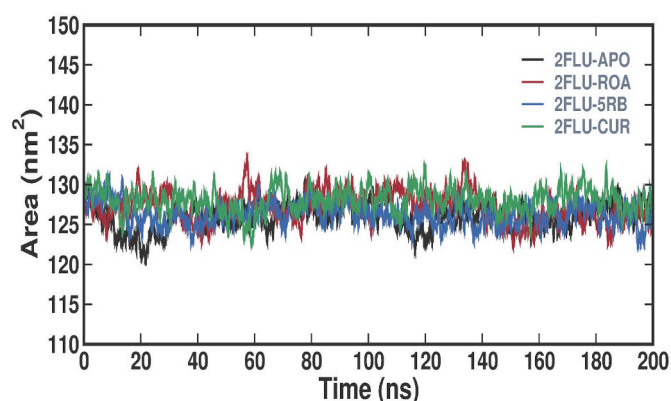**Fig. 5.** A comparison of the Rg values of the 2FLU-APO, 2FLU-ROA, 2FLU-5RB, and 2FLU-CUR complex.

Fig. 6. A comparison of the SASA values of the 2FLU-APO, 2FLU-ROA, 2FLU-5RB, and 2FLU-CUR complex.

Fig. 7. Intramolecular hydrogen bonds during the simulation time.

Fig. 8. Intermolecular hydrogen bonds form between the protein and ligand throughout the simulation period.

Fig. 9. The 2D projection graphic illustrates the conformation sampling of 2FLU-APO, 2FLU-ROA, 2FLU-5RB, and 2FLU-CUR complex on PC1 and PC2.

3.3.2. Root mean square fluctuation (RMSF)

RMSF quantifies the variability of individual residues and flexible regions within a protein throughout MDS. Compact protein structures like sheets and helices have lower RMSFs, whereas loosely organized loop regions display larger RMSF values [66]. This investigation involved calculating and graphing the RMSF values for each residue in the 2FLU-APO, 2FLU-ROA, 2FLU-5RB, and 2FLU-CUR complexes (Fig. 5). The average RMSF values for 2FLU-APO, 2FLU-ROA, 2FLU-5RB, and 2FLU-CUR were found to be 0.09 ± 0.04 nm, 0.09 ± 0.05 nm, 0.09 ± 0.04 nm and 0.10 ± 0.06 nm. The findings suggest that the 2FLU-ROA complex had no significant impact on the overall distribution of RMSF (Fig. 4).

3.3.3. Radius of gyration (Rg)

To evaluate the dynamic stability and compactness of 2FLU-APO, 2FLU-ROA, 2FLU-5RB, and 2FLU-CUR, we calculated the Rg values and plotted them over time (Fig. 5). The average Rg values for 2FLU-APO, 2FLU-ROA, 2FLU-5RB and 2FLU-CUR were found to be 1.78 ± 0.01 nm, 1.79 ± 0.01 nm, 1.79 ± 0.006 nm and 1.79 ± 0.007 nm.

3.3.4. Solvent accessible surface area (SASA)

SASA is utilized to assess the accessibility of a protein molecule inside a solvent environment [66]. The investigation involved calculating and graphing the SASA values to analyze how the binding of 2FLU-ROA affects the solvent accessibility of the target (Fig. 6). The SASA values demonstrate consistent equilibration without notable changes throughout the simulation. The average SASA values for 2FLU-APO, 2FLU-ROA, 2FLU-5R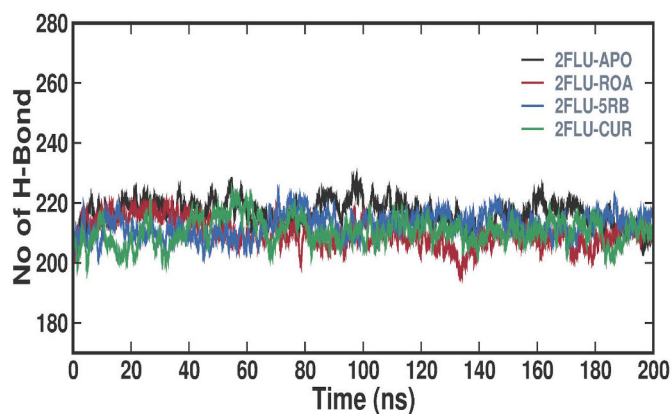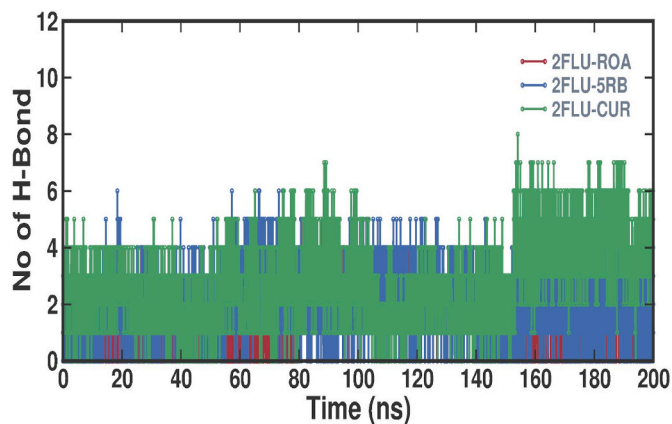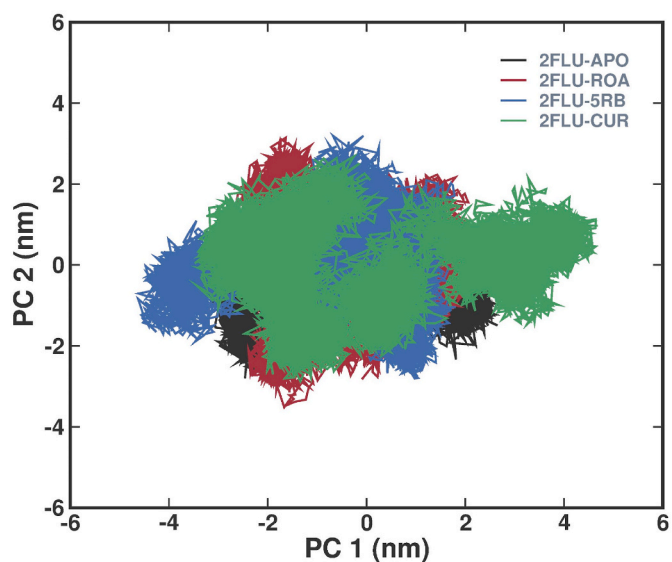B and 2FLU-CUR were found to be 125.93 ± 2.29 nm^2, 127.22 ± 2.51 nm^2, 126.23 ± 2.18 nm^2 and 128.05 ± 2.2 nm^2.

3.3.5. Intra and inter hydrogen bond

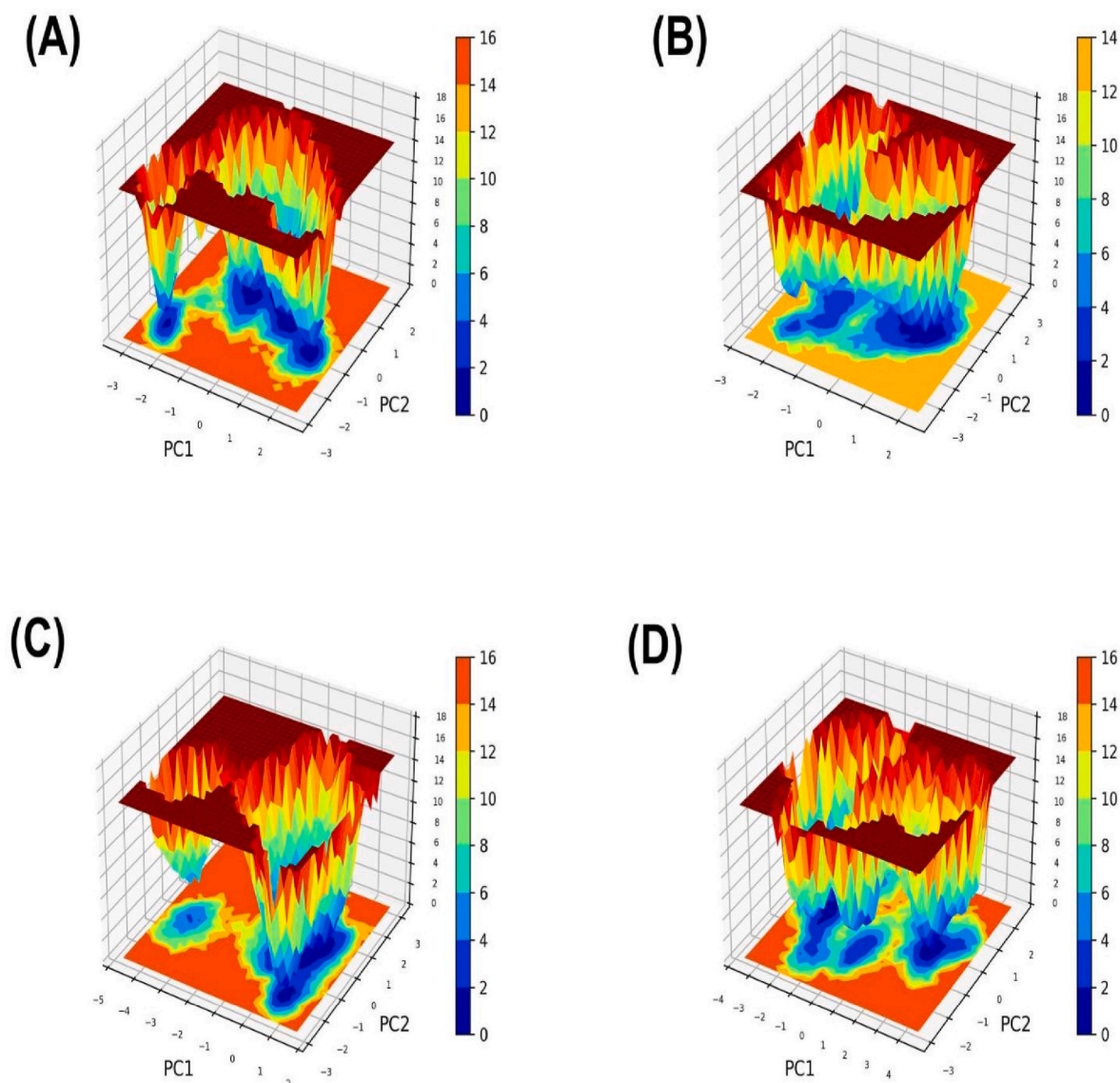The presence of intra- and inter-hydrogen bonds portrays an

Fig. 10. The free energy landscape plots for (A) 2FLU-APO, (B) 2FLU-ROA, (C) 2FLU-5RB, and (D) 2FLU-CUR Complex.

important function in determining the stability of 2FLU-APO, 2FLU-ROA, 2FLU-5RB, and 2FLU-CUR interactions. This work examined the temporal characteristics of the intra-hydrogen bonds of the complexes (Fig. 7). The intramolecular hydrogen bonding confirmed the stability of the protein structure after ROA binding. We found that ROA did not appear to disrupt the hydrogen bonding within the protein. Hydrogen

bonds have a crucial role in establishing the stability of interactions between proteins and ligands. The formation of intermolecular hydrogen bonds between the protein and the ligand throughout the simulation period is clearly observed (Fig. 8). The 2FLU-ROA complex remained stable during the simulation period with a minimum of 2-5 intermolecular hydrogen bonds.

3.3.6. Principal component analysis (PCA)

We performed PCA to investigate the collective movements in 2FLU-APO, 2FLU-ROA, 2FLU-5RB, and 2FLU-CUR. We used PCA to investigate the conformational dynamics of 2FLU-APO, 2FLU-ROA, 2FLU-5RB, and 2FLU-CUR throughout the simulation (Fig. 9). PCA analysis indicates that the 2FLU-ROA complex experienced a decrease in overall flexibility on both eigenvectors, suggesting increased stability. The plot illustrates that the 2FLU-ROA complex effectively covered and coincided with nearly all of the conformational movements. Overall, the reduced level of movements seen in the 2FLU-ROA indicates that 2FLU-ROA had minimal impact on the target conformation and dynamics, hence confirming the stability of the complex.

3.3.7. Free energy landscapes (FELs)

Examining the FELs is a widely used method for studying the

Table 3

2FLU-ROA has a van der Waals energy of −100.192±5.321 kJ/mol, an electrostatic energy of −24.221±9.139 kJ/mol, polar solvation energy of 66.388 ±9.412 kJ/mol, and a binding energy of −70.987±10.186 kJ/mol.

System	Van der Waal energy	Electrostatic energy	Polar solvation energy	Binding energy
2FLU-ROA	−100.192 ±5.321 kJ/ mol	−24.221±9.139 kJ/mol	66.388 ±9.412 kJ/ mol	−70.987 ±10.186 kJ/ mol
2FLU-5RB	−264.008 ±14.991 kJ/ mol	−40.033±6.010 kJ/mol	166.436 ±8.107 kJ/ mol	−163.620 ±18.792 kJ/ mol
2FLU-CUR	−199.822 ±21.753 kJ/ mol	−57.816 ±13.290 kJ/mol	184.099 ±9.791 kJ/ mol	−94.831 ±12.972 kJ/ mol

processes and overall stability of protein folding. The most stable conformational ensembles for a protein structure are depicted in FEL diagrams [66]. In this study, we produced FEL plots for PC1 and PC2, where darker blue areas represent a more stable protein conformation with lower energy (Fig. 10). The FEL plot indicate the stability of the 2FLU-ROA complex.

3.3.8. MM – PBSA

A comparison of the van der Waals energy, Electrostatic energy, Polar solvation energy, and Binding energy of 2FLU-ROA, 2FLU-5RB, and 2FLU-CUR, was determined using the MM-PBSA approach (Table 3). We calculated the individual contributions of each residue to the interaction energy during a steady simulation trajectory.

4. Conclusions

The Nrf2 signaling pathway represents an innovative therapeutic target in the testis, and further research is necessary to elucidate the function of this Nrf2 pathway in suppressing oxidative stress in the testicles. Moreover, there has been a lack of thorough investigation into the clinical trials on the impact of the Nrf2 signaling pathway on human testes. Further investigation is required to examine the optimal dosage and duration of treatment to determine the significance of Nrf2 activation. This current study shows that ROA can be a potent Nrf2 activator by exhibiting inhibitory activity against the Keap1 protein. The present research shows that ROA can be a potent drug candidate choice against arsenic-induced male reproductive toxicity as it successfully combats oxidative stress. More research is required to understand and enhance ROA's potential as an antioxidant.

Funding

This work did not receive any funding.

Ethics approval and consent to participate

Not applicable.

CRediT authorship contribution statement

Anirban Goutam Mukherjee: Writing – review & editing, Writing – original draft, Visualization, Validation, Software. **Abilash Valsala Gopalakrishnan:** Writing – review & editing, Writing – original draft, Visualization, Validation, Supervision, Software, Resources, Project administration, Methodology, Investigation, Funding acquisition, Formal analysis, Data curation, Conceptualization.

Declaration of competing interest

The authors declare that they have no known competing financial interests or personal relationships that could have appeared to influence the work reported in this paper.

Data availability

Data will be made available on request.

Acknowledgments

References

[1] J. Aitken, H. Fisher, Reactive oxygen species generation and human spermatozoa: the balance of benefit and risk, Bioessays 16 (4) (Apr 1994) 259–267 (in eng).
[2] M. Valko, D. Leibfritz, J. Moncol, M.T. Cronin, M. Mazur, J. Telser, Free radicals and antioxidants in normal physiological functions and human disease, Int. J. Biochem. Cell Biol. 39 (1) (2007) 44–84 (in eng).
[3] R.J. Aitken, M.A. Baker, D. Sawyer, Oxidative stress in the male germ line and its role in the aetiology of male infertility and genetic disease, Reprod. Biomed. Online 7 (1) (Jul-Aug 2003) 65–70 (in eng).
[4] R.J. Aitken, M.A. Baker, Oxidative stress, sperm survival and fertility control, Mol. Cell. Endocrinol. 250 (1–2) (May 16 2006) 66–69 (in eng).
[5] A. Agarwal, G. Virk, C. Ong, S.S. du Plessis, Effect of oxidative stress on male reproduction, World J Mens Health 32 (1) (Apr 2014) 1–17 (in eng).
[6] S. Venkatesh, M.B. Shamsi, D. Deka, V. Saxena, R. Kumar, R. Dada, Clinical implications of oxidative stress & sperm DNA damage in normozoospermic infertile men, Indian J. Med. Res. 134 (3) (Sep 2011) 396–398 (in eng).
[7] A. Agarwal, S. Prabakaran, S. Allamaneni, What an andrologist/urologist should know about free radicals and why, Urology 67 (1) (Jan 2006) 2–8 (in eng).
[8] S. Bisht, M. Faiq, M. Tolahunase, R. Dada, Oxidative stress and male infertility, Nat. Rev. Urol. 14 (8) (Aug 2017) 470–485 (in eng).
[9] R.J. Aitken, Z. Gibb, L.A. Mitchell, S.R. Lambourne, H.S. Connaughton, G.N. De Iuliis, Sperm motility is lost in vitro as a consequence of mitochondrial free radical production and the generation of electrophilic aldehydes but can be significantly rescued by the presence of nucleophilic thiols, Biol. Reprod. 87 (5) (Nov 2012) 110 (in eng).
[10] E. de Lamirande, C. Gagnon, Reactive oxygen species and human spermatozoa. I. Effects on the motility of intact spermatozoa and on sperm axonemes, J. Androl. 13 (5) (Sep-Oct 1992) 368–378 (in eng).
[11] K. Mar Wai, M. Umezaki, O. Mar, M. Umemura, C. Watanabe, Arsenic exposure through drinking Water and oxidative stress Status: a cross-sectional study in the Ayeyarwady region, Myanmar, J. Trace Elem. Med. Biol. 54 (Jul 2019) 103–109 (in eng).
[12] I. Palma-Lara, et al., Arsenic exposure: a public health problem leading to several cancers, Regul. Toxicol. Pharmacol. 110 (Feb 2020) 104539 (in eng).
[13] B.C. Minatel, et al., Environmental arsenic exposure: from genetic susceptibility to pathogenesis, Environ. Int. 112 (Mar 2018) 183–197 (in eng).
[14] F.L. Muller, Y. Liu, H. Van Remmen, Complex III releases superoxide to both sides of the inner mitochondrial membrane, J. Biol. Chem. 279 (47) (Nov 19 2004) 49064–49073 (in eng).
[15] D. Mishra, A. Mehta, S.J. Flora, Reversal of arsenic-induced hepatic apoptosis with combined administration of DMSA and its analogues in Guinea pigs: role of glutathione and linked enzymes, Chem. Res. Toxicol. 21 (2) (Feb 2008) 400–407 (in eng).
[16] M. Machado-Neves, Effect of heavy metals on epididymal morphology and function: an integrative review, Chemosphere 291 (Pt 2) (Mar 2022) 133020 (in eng).
[17] A.C.F. Souza, et al., Effects of sodium arsenite and arsenate in testicular histomorphometry and antioxidants enzymes activities in rats, Biol. Trace Elem. Res. 171 (2) (Jun 2016) 354–362 (in eng).
[18] M. Zubair, M. Ahmad, Z.I. Qureshi, Review on arsenic-induced toxicity in male reproductive system and its amelioration, Andrologia 49 (9) (Nov 2017) (in eng).
[19] A.G. Mukherjee, A. Valsala Gopalakrishnan, The interplay of arsenic, silymarin, and NF-κB pathway in male reproductive toxicity: a review, Ecotoxicol. Environ. Saf. 252 (Mar 1 2023) 114614 (in eng).
[20] Y.J. Kim, J.M. Kim, Arsenic toxicity in male reproduction and development, Dev Reprod 19 (4) (Dec 2015) 167–180 (in eng).
[21] Q. Zeng, H. Yi, L. Huang, Q. An, H. Wang, Reduced testosterone and Ddx3y expression caused by long-term exposure to arsenic and its effect on spermatogenesis in mice, Environ. Toxicol. Pharmacol. 63 (Oct 2018) 84–91 (in eng).
[22] M.M. Ommati, et al., Paternal exposure to arsenic resulted in oxidative stress, autophagy, and mitochondrial impairments in the HPG axis of pubertal male offspring, Chemosphere 236 (Dec 2019) 124325 (in eng).
[23] Y. Aydin, B. Orta-Yilmaz, Synergistic effects of arsenic and fluoride on oxidative stress and apoptotic pathway in Leydig and Sertoli cells, Toxicology 475 (Jun 15 2022) 153241 (in eng).
[24] Y.J. Park, M.G. Pang, Mitochondrial functionality in male fertility: from spermatogenesis to fertilization, Antioxidants 10 (1) (Jan 12 2021) (in eng).
[25] H. Chen, et al., Toxic effects of arsenic trioxide on spermatogonia are associated with oxidative stress, mitochondrial dysfunction, autophagy and metabolomic alterations, Ecotoxicol. Environ. Saf. 190 (Mar 1 2020) 110063 (in eng).
[26] Y. Han, et al., Arsenic influences spermatogenesis by disorganizing the elongation of spermatids in adult male mice, Chemosphere 238 (Jan 2020) 124650 (in eng).
[27] Y. Han, et al., Chronic arsenic exposure lowered sperm motility via impairing ultra-microstructure and key proteins expressions of sperm acrosome and flagellum formation during spermiogenesis in male mice, Sci. Total Environ. 734 (Sep 10 2020) 139233 (in eng).
[28] A.T. de Araújo-Ramos, et al., The endocrine disrupting effects of sodium arsenite in the rat testis is not mediated through macrophage activation, Reprod. Toxicol. 102 (Jun 2021) 1–9 (in eng).
[29] D.D. Zhang, M. Hannink, Distinct cysteine residues in Keap1 are required for Keap1-dependent ubiquitination of Nrf2 and for stabilization of Nrf2 by chemopreventive agents and oxidative stress, Mol. Cell Biol. 23 (22) (Nov 2003) 8137–8151 (in eng).

[30] I.D. Boyenle, et al., Direct Keap1-kelch inhibitors as potential drug candidates for oxidative stress-orchestrated diseases: a review on in silico perspective, Pharmacol. Res. 167 (May 2021) 105577 (in eng).

[31] H. Kumar, I.S. Kim, S.V. More, B.W. Kim, D.K. Choi, Natural product-derived pharmacological modulators of Nrf2/ARE pathway for chronic diseases, Nat. Prod. Rep. 31 (1) (Jan 2014) 109–139 (in eng).

[32] T.I. Adelusi, et al., Keap1/Nrf2/ARE signaling unfolds therapeutic targets for redox imbalanced-mediated diseases and diabetic nephropathy, Biomed. Pharmacother. 123 (Mar 2020) 109732 (in eng).

[33] K. Taguchi, H. Motohashi, M. Yamamoto, Molecular mechanisms of the Keap1–Nrf2 pathway in stress response and cancer evolution, Gene Cell. 16 (2) (Feb 2011) 123–140 (in eng).

[34] A.G. Mukherjee, A.V. Gopalakrishnan, The mechanistic insights of the antioxidant Keap1-Nrf2 pathway in oncogenesis: a deadly scenario, Med. Oncol. 40 (9) (Jul 22 2023) 248 (in eng).

[35] V. Ngo, M.L. Duennwald, Nrf2 and oxidative stress: a general overview of mechanisms and implications in human disease, Antioxidants 11 (12) (Nov 27 2022) (in eng).

[36] M. Rojo de la Vega, E. Chapman, D.D. Zhang, NRF2 and the hallmarks of cancer, Cancer Cell 34 (1) (Jul 9 2018) 21–43 (in eng).

[37] A.M. Shahat, G. Rizzoto, J.P. Kastelic, Amelioration of heat stress-induced damage to testes and sperm quality, Theriogenology 158 (Dec 2020) 84–96 (in eng).

[38] A. Wajda, et al., Nuclear factor E2-related factor-2 (Nrf2) expression and regulation in male reproductive tract, Pharmacol. Rep. 68 (1) (Feb 2016) 101–108 (in eng).

[39] X. Jiang, Y. Bai, Z. Zhang, Y. Xin, L. Cai, Protection by sulforaphane from type 1 diabetes-induced testicular apoptosis is associated with the up-regulation of Nrf2 expression and function, Toxicol. Appl. Pharmacol. 279 (2) (Sep 1 2014) 198–210 (in eng).

[40] S.H. Yang, et al., Protective role of curcumin in cadmium-induced testicular injury in mice by attenuating oxidative stress via Nrf2/ARE pathway, Environ. Sci. Pollut. Res. Int. 26 (33) (Nov 2019) 34575–34583 (in eng).

[41] D.E. Rotimi, O.A. Ojo, T.D. Olaolu, O.S. Adeyemi, Exploring Nrf2 as a therapeutic target in testicular dysfunction, Cell Tissue Res. 390 (1) (Oct 2022) 23–33 (in eng).

[42] J. Moreno-Fernandez, M.J.M. Alférez, I. López-Aliaga, J. Diaz-Castro, Protective effects of fermented goat milk on genomic stability, oxidative stress and inflammatory signalling in testis during anaemia recovery, Sci. Rep. 9 (1) (Feb 19 2019) 2232 (in eng).

[43] Y. Li, et al., Protective effects of nuclear factor erythroid 2-related factor 2 on whole body heat stress-induced oxidative damage in the mouse testis, Reprod. Biol. Endocrinol. 11 (Mar 21 2013) 23 (in eng).

[44] S.G. Li, et al., Lutein alleviates arsenic-induced reproductive toxicity in male mice via Nrf2 signaling, Hum. Exp. Toxicol. 35 (5) (May 2016) 491–500 (in eng).

[45] L. He, et al., Protective effects of proanthocyanidins against cadmium-induced testicular injury through the modification of Nrf2-Keap1 signal path in rats, Environ. Toxicol. Pharmacol. 57 (Jan 2018) 1–8 (in eng).

[46] C.E. Guerrero-Beltrán, M. Calderón-Oliver, J. Pedraza-Chaverri, Y.I. Chirino, Protective effect of sulforaphane against oxidative stress: recent advances, Exp. Toxicol. Pathol. 64 (5) (Jul 2012) 503–508 (in eng).

[47] Y. Wang, et al., Sulforaphane reduction of testicular apoptotic cell death in diabetic mice is associated with the upregulation of Nrf2 expression and function, Am. J. Physiol. Endocrinol. Metab. 307 (1) (Jul 1 2014) E14–E23 (in eng).

[48] Y. Zhao, et al., Lycopene prevents DEHP-induced Leydig cell damage with the Nrf2 antioxidant signaling pathway in mice, J. Agric. Food Chem. 68 (7) (Feb 19 2020) 2031–2040 (in eng).

[49] R. Foresti, M. Hoque, D. Monti, C.J. Green, R. Motterlini, Differential activation of heme oxygenase-1 by chalcones and rosolic acid in endothelial cells, J. Pharmacol. Exp. Therapeut. 312 (2) (Feb 2005) 686–693 (in eng).

[50] K.N. Amin, R. Palanisamy, D.V.L. Sarada, D. Ali, T. Suzuki, K.M. Ramkumar, "Effect of Rosolic acid on endothelial dysfunction under ER stress in pancreatic microenvironment," Free Radic. Res. 55 (6) (Jun 2021) 698–713 (in eng).

[51] V. Consoli, V. Sorrenti, I. Burò, M.N. Modica, L. Vanella, Antiproliferative effect of plant-derived bioactive compounds endowed with antioxidant activity on breast cancer cells, Nutraceuticals 2 (3) (2022) 246–252.

[52] E. Crisman, et al., KEAP1-NRF2 protein-protein interaction inhibitors: design, pharmacological properties and therapeutic potential, Med. Res. Rev. 43 (1) (Jan 2023) 237–287 (in eng).

[53] S.H. Shahcheraghi, et al., Nrf2 regulation by curcumin: molecular aspects for therapeutic prospects, Molecules 27 (1) (Dec 28 2021) (in eng).

[54] V.P. Menon, A.R. Sudheer, Antioxidant and anti-inflammatory properties of curcumin, Adv. Exp. Med. Biol. 595 (2007) 105–125 (in eng).

[55] R. Mohebbati, A. Anaeigoudari, M.R. Khazdair, "The effects of Curcuma longa and curcumin on reproductive systems," Endocr. Regul. 51 (4) (Oct 26 2017) 220–228 (in eng).

[56] M. Lonare, et al., Evaluation of ameliorative effect of curcumin on imidacloprid-induced male reproductive toxicity in wistar rats, Environ. Toxicol. 31 (10) (Oct 2016) 1250–1263 (in eng).

[57] A. Daina, O. Michielin, V. Zoete, SwissADME: a free web tool to evaluate pharmacokinetics, drug-likeness and medicinal chemistry friendliness of small molecules, Sci. Rep. 7 (Mar 3 2017) 42717 (in eng).

[58] B.S. Gangadharappa, R. Sharath, P.D. Revanasiddappa, V. Chandramohan, M. Balasubramaniam, T.P. Vardhineni, Structural insights of metallo-beta-lactamase revealed an effective way of inhibition of enzyme by natural inhibitors, J. Biomol. Struct. Dyn. 38 (13) (Aug 2020) 3757–3771 (in eng).

[59] R. Kumari, R. Kumar, A. Lynn, g_mmpbsa–a GROMACS tool for high-throughput MM-PBSA calculations, J. Chem. Inf. Model. 54 (7) (Jul 28 2014) 1951–1962 (in eng).

[60] M.C. Lu, J.A. Ji, Z.Y. Jiang, Q.D. You, The keap1-Nrf2-ARE pathway as a potential preventive and therapeutic target: an update, Med. Res. Rev. 36 (5) (Sep 2016) 924–963 (in eng).

[61] A. Akmal, A. Javaid, R. Hussain, A. Kanwal, M. Zubair, U.A. Ashfaq, Screening of phytochemicals against Keap1- NRF2 interaction to reactivate NRF2 Functioning: pharmacoinformatics based approach (in eng), Pak. J. Pharm. Sci. 32 (6) (Nov 2019) 2823–2828 (Supplementary).

[62] A. Daina, V. Zoete, A BOILED-egg to predict gastrointestinal absorption and brain penetration of small molecules, ChemMedChem 11 (11) (Jun 6 2016) 1117–1121 (in eng).

[63] F. Montanari, G.F. Ecker, Prediction of drug-ABC-transporter interaction–Recent advances and future challenges, Adv. Drug Deliv. Rev. 86 (Jun 23 2015) 17–26 (in eng).

[64] C.A. Lipinski, F. Lombardo, B.W. Dominy, P.J. Feeney, Experimental and computational approaches to estimate solubility and permeability in drug discovery and development settings, Adv. Drug Deliv. Rev. 46 (1–3) (Mar 1 2001) 3–26 (in eng).

[65] A. Daina, O. Michielin, V. Zoete, iLOGP: a simple, robust, and efficient description of n-octanol/water partition coefficient for drug design using the GB/SA approach, J. Chem. Inf. Model. 54 (12) (Dec 22 2014) 3284–3301 (in eng).

[66] G.C.L. Priyanka, et al., Tanshinone IIA from Salvia miltiorrhiza alleviates follicular maturation arrest symptoms in zebrafish via binding to the human androgen receptors and modulating Tox3 and Dennd1a, Tissue Cell 88 (May 7 2024) 102404 (in eng).